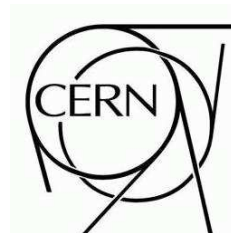


ATLAS NOTE

February 2, 2008



Track Based Alignment of the ATLAS Silicon Detectors with the Robust Alignment Algorithm

Florian Heinemann
University of Oxford
f.heinemann1@physics.ox.ac.uk

Abstract

The Robust Alignment algorithm for the ATLAS silicon detectors is presented. It is an iterative method based on centering residual and overlap residual distributions. Tests on simulated and real data are discussed.

Contents

1	Introduction	2
2	ATLAS Coordinate Frames	3
3	Residuals and Overlap Residuals	3
4	Main Principle	3
5	Calculation of Alignment Constants	4
6	Uncertainties on Alignment Constants	6
7	Distributed Alignment	7
8	Sagitta Distortions	7
9	Removal of Edge Channels	8
10	Effect of Multiple Scattering on SCT Local Y Residuals	9
11	Combined Test Beam Alignment	10
12	SCT Alignment With Cosmic Ray Tracks	10
13	CSC Alignment	11
14	Summary and Conclusion	12
15	Acknowledgements	13

1 Introduction

Alignment of ever larger silicon tracking systems in modern high energy physics experiments is very challenging. Due to the raising numbers of degrees of freedom, traditional alignment algorithms based on χ^2 minimisation face increasing numerical difficulties. A simple, independent and robust alignment algorithm is crucial for a quick and reliable calculation of alignment constants. Furthermore, it is important to have an alternative alignment method in order to cross-check results from χ^2 minimisation algorithms, especially during early data taking when the experimental environment is not yet well known.

The ATLAS silicon tracking system [1] consists of two subsystems: the silicon pixel detector (PIXEL) with 1744 individual modules and the semi-conductor tracker (SCT) which is made of 4088 two-sided silicon strip detectors. Each of the subsystems are divided in one barrel and two endcap detectors.

In this paper the Robust Alignment algorithm and various tests on real and simulated data are presented. The main advantage of this algorithm over other track based alignment methods is its simplicity and robustness. The Robust Alignment is limited to the alignment of only two to three out of six degrees of freedom per module.

2 ATLAS Coordinate Frames

To describe the ATLAS detector various coordinate frames are used. In this paper the local coordinate frames defined for each silicon module are mainly used. The origin of each Cartesian right-handed frame is in the centre of the module. Local Y is parallel to the beam pipe for PIXEL barrel modules and perpendicular to the beam pipe for PIXEL endcap modules. For SCT modules, local Y is parallel to the centre silicon strip. The local X coordinate is always in the module plane and perpendicular to the local Y coordinate, and is the direction in which the silicon modules have the best spatial resolution. The local Z coordinate is thus perpendicular to the module plane by construction. It always points away from the interaction point.

3 Residuals and Overlap Residuals

The Robust Alignment algorithm is based on residual and overlap residual measurements. Residuals are defined as the difference between the hit and the track position in the plane of the module. The PIXEL detector measures the hit position directly in both the local X and Y direction. As the SCT is a strip detector, the local Y hit position must be calculated from two crossing strips and the track direction. All residuals are defined in the local frame of the module. In general, residuals may be biased or unbiased. Biased residuals show the difference between the hit and the track position if the track is fitted to all its hits, whereas unbiased residuals are calculated after removing the respective hit and refitting the track.

Overlap residuals are defined as the difference between two residuals from two overlapping modules (Fig. 1). There are two types of residuals, residuals in local X and Y, and two types of overlaps, overlaps in the local X and Y direction. Thus, four different overlap residuals can be constructed. The naming convention is $ovres_{AB}$ where A is the residual type and B the overlap type. Obviously, SCT overlap residuals in local Y are only defined if in each module two crossing strips are hit by a particle.

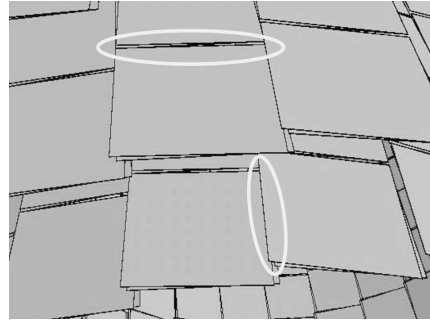


Figure 1: Overlapping silicon modules

4 Main Principle

The Robust Alignment algorithm is based on two main premises:

- ◇ For a perfectly aligned detector all residual and overlap residual distributions are centred around zero.
- ◇ If only one module is shifted by δx in the direction of the residual measurement, the mean of its unbiased residual and overlap residual distribution is equal to $-\delta x$.

If all modules are misaligned, correlations have to be taken into account. This algorithm automatically correlates modules within one ring or stave through using overlap residuals. Dependencies on modules which are positioned further away in the detector are taken into account through an iterative procedure. Using overlap residuals it is also possible to take advantage of a third principle:

- ◇ The change of circumference - and thus the average radial shift of each module - in a ring of overlapping modules is proportional to the sum of overlap residuals in the ring.

If the circumference of a detector ring is at the design value, the sum of overlap residuals vanishes even if the modules are generally misaligned. However, a positive (negative) sum means that all modules are systematically shifted away from (towards) each other which can only be explained with an increased (decreased) circumference. In Fig. 2 the change in the mean overlap residuals is shown if the radius of a detector ring is increased by 50 μm . The measurement of deviations in the radial direction is not straight forward for other types of algorithms, as tracks enter the silicon modules mostly perpendicularly. The Robust Alignment algorithm does not measure module rotations. Furthermore, it is assumed that the modules do not deform and that the SCT wafers do not move with respect to each other.

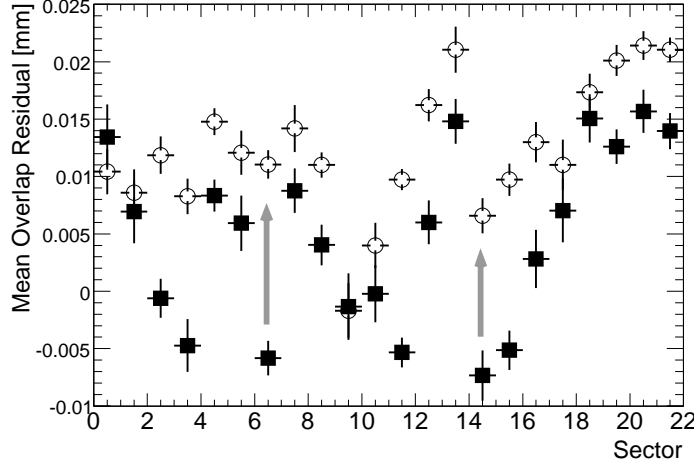


Figure 2: Mean overlap residuals for all modules in a PIXEL ring where the modules are randomly misaligned: A geometry with nominal radius (black squares) and with a radius increased by 50 μm (white circles) are shown.

5 Calculation of Alignment Constants

The relative alignment shifts for each module, a^X , a^Y and a^Z , are determined from the residual and overlap residual measurements. A shift in the mean of the residual distribution of a module and a shift in the mean of the overlap residual distributions is a measure of the same quantity; the displacement of the module. For each local coordinate, X and Y, there is one residual distribution and a maximum of two overlap residual distributions. It is natural to combine these up to three measurements respecting their statistical uncertainties:

$$a^{X/Y} = - \sum_{j=1}^n \frac{s_j^{X/Y}}{(\delta s_j^{X/Y})^2} / \sum_{j=1}^n \frac{1}{(\delta s_j^{X/Y})^2}, \quad n \leq 3. \quad (1)$$

The first summand in this equation comes from the residual measurements of each module. As these are directly correlated with the module displacement, $s_1^{X/Y}$ is given by the mean of the module's residual distribution:

$$s_1^{X/Y} = \overline{res}_{X/Y}. \quad (2)$$

Thus, the first summand is given by:

$$\frac{s_1^{X/Y}}{(\delta s_1^{X/Y})^2} = \frac{\overline{res}_{X/Y}}{\delta \overline{res}_{X/Y}^2} \quad (3)$$

The statistical uncertainty on the mean residual $\delta\overline{res}_{X/Y}$ is given by the RMS of the residual distribution and its number of entries:

$$\delta\overline{res}_{X/Y} = \frac{RMS_{res}}{\sqrt{n_{Hits}}}, \quad (4)$$

If the module has a local X (local Y) overlap to a neighbouring module the second (third) term has to be considered as well. Overlap residuals are also correlated to the displacement of a module. Furthermore, overlap residual distributions are dependent on displacements of the neighbouring modules. Therefore, these correlations have to be accounted for in the calculations of the alignment constants. From the overlap point of view, where to set the starting point in a ring or stave is an arbitrary choice. The Robust Alignment algorithm begins with the modules which have the smallest sector or ring number. All other module position measurements from the overlap residuals are performed with respect to the neighbour with the smallest sector or ring number:

$$s_2^X = \sum_{i=0}^{i=N_s} \overline{ovres}_{XX} \quad (5)$$

$$s_3^Y = \sum_{i=0}^{i=N_r} \overline{ovres}_{YY} \quad (6)$$

Here, N_s is the sector number and N_r the ring number of the module to be aligned. An average increase or decrease in the overall circumference of a detector ring leads to a systematically positive or negative bias in the sum of all overlap residuals. If a detector ring is complete and all overlap residuals are measured with sufficient precision the algorithm is able to perform corrections in the local Z direction:

$$a^Z = -\frac{\sum_{i=0}^{i=N_a} \overline{ovres}_{XX}}{2\pi} \quad (7)$$

Here, N_a is the number of all modules in the ring of the module to be aligned. However, this bias needs to be removed from s_2^X in the case of local X local X overlap residuals:

$$s_2^X = \sum_{i=0}^{i=N_s} \overline{ovres}_{XX} + \frac{2\pi a^Z}{N_a} \quad (8)$$

Thus, for local X measurements the second and third term in Eq. 1 is given by:

$$\frac{s_2^X}{(\delta s_2^X)^2} = \frac{\sum_{i=0}^{i=N_s} \overline{ovres}_{XX} + \frac{2\pi a^Z}{N_a}}{\delta(\sum_{i=0}^{i=N_s} \overline{ovres}_{XX} + \frac{2\pi a^Z}{N_a})^2} \quad (9)$$

$$\frac{s_3^X}{(\delta s_3^X)^2} = \frac{\overline{ovres}_{XY}}{\delta \overline{ovres}_{XY}^2} \quad (10)$$

As the detector shape is a cylinder, rather than a sphere, there is no 2π -symmetry for the detector staves. Therefore, this correction is not applied for shifts in the local Y direction. The second and third term in Eq. 1 for the calculation of the local Y misalignments are given by:

$$\frac{s_2^Y}{(\delta s_2^Y)^2} = \frac{\overline{ovres}_{YX}}{\delta \overline{ovres}_{YX}^2} \quad (11)$$

$$\frac{s_3^Y}{(\delta s_3^Y)^2} = \frac{\sum_{i=0}^{i=N_r} \overline{ovres}_{YY}}{\delta(\sum_{i=0}^{i=N_r} \overline{ovres}_{YY})^2} \quad (12)$$

The alignment constants are finally given by the following equations:

$$a^X = - \frac{\frac{\overline{res}_X}{\delta \overline{res}_X^2} + \frac{\sum_{i=0}^{i=N_s} \overline{ovres}_{XX} + \frac{2\pi a^Z}{N_a}}{\delta (\sum_{i=0}^{i=N_s} \overline{ovres}_{XX} + \frac{2\pi a^Z}{N_a})^2} + \frac{\overline{ovres}_{XY}}{\delta \overline{ovres}_{XY}^2}}{N^X} \quad (13)$$

$$a^Y = - \frac{\frac{\overline{res}_Y}{\delta \overline{res}_Y^2} + \frac{\overline{ovres}_{YX}}{\delta \overline{ovres}_{YX}^2} + \frac{\sum_{i=0}^{i=N_r} \overline{ovres}_{YY}}{\delta (\sum_{i=0}^{i=N_r} \overline{ovres}_{YY})^2}}{N^Y} \quad (14)$$

$$a^Z = - \frac{\sum_{i=0}^{i=N_a} \overline{ovres}_{XX}}{2\pi} \quad (15)$$

The normalisations N^X and N^Y are defined as

$$N^X = \frac{1}{\delta \overline{res}_X^2} + \frac{1}{\delta (\sum_{i=0}^{i=N_s} \overline{ovres}_{XX} + \frac{2\pi a^Z}{N_a})^2} + \frac{1}{\delta \overline{ovres}_{XY}^2} \quad (16)$$

$$N^Y = \frac{1}{\delta \overline{res}_Y^2} + \frac{1}{\delta \overline{ovres}_{YX}^2} + \frac{1}{\delta (\sum_{i=0}^{i=N_r} \overline{ovres}_{YY})^2} \quad (17)$$

The alignment corrections are obtained in the local X, Y and Z coordinates. Therefore, from the residual and overlap residual point of view there is no difference between the barrel and the endcaps, and the same calculations are used for both parts of the detector. For large misalignments, applying damping factors to the alignment constant calculation leads to a smoother convergence.

6 Uncertainties on Alignment Constants

Statistical uncertainties on the alignment constants are determined by the uncertainties on the mean values of the residual and overlap residual distributions which are each given by

$$\delta_{mean} = \frac{RMS}{\sqrt{n_{Hits}}}, \quad (18)$$

with n_{Hits} being the number of hits in that particular distribution. Therefore, the exact uncertainty on each module shift depends on the width of the measured distributions and on the illumination of the module. The overall statistical uncertainties for each of the three coordinates are given by:

$$\delta a^X = \frac{1}{\sqrt{N^X}} \quad (19)$$

$$\delta a^Y = \frac{1}{\sqrt{N^Y}} \quad (20)$$

$$\delta a^Z = \frac{\sqrt{\sum_{i=0}^{i=N_a} \delta \overline{ovres}_{XX}^2}}{2\pi} \quad (21)$$

N^X and N^Y are defined in Eq. 16 and 17. The number of hits per module N_{HpM} required to reach a certain statistical uncertainty Δ can be estimated by

$$N_{HpM} = \frac{1}{\Delta^2 \times \left(\frac{1}{RMS_{res}^2} + \frac{2}{G \times RMS_{ovres}^2} \right)}. \quad (22)$$

Here, RMS_{res} and RMS_{ovres} represent the average RMS for the residual and overlap residual distributions. The geometrical factor G corrects for two considerations. Firstly, depending on the location of the

module in the detector, there are about ten times fewer overlap residuals than residuals. Secondly, some overlap residual measurements are correlated with others in the same ring or stave. The uncertainties of these measurements have to be also taken into account. Thus, G is defined as the product of the number of correlated measurements and the ratio of residual to overlap residual measurements. Values for G are typically between 10 and 300. With each iteration, the residual and overlap residual distributions generally become narrower and the tracking efficiency is improved. Thus, the statistical uncertainties improve significantly with each iteration. On the whole, the PIXEL detector provides a much better intrinsic resolution compared to the SCT, leading to more precise alignment constants. Furthermore, the number of hits per module increase with smaller layer numbers. Hence, the innermost layers are expected to have the best precision.

The Robust Alignment constants have three types of additional errors which are typical for track based alignment. First of all the residual measurement has a statistical uncertainty in itself. Both the hit position and the track position measurements have an associated error. However, these errors are symmetric with respect to the residual measurement. Therefore, the alignment constant calculation is not affected by this uncertainty. Secondly, there are certain global modes which are not determined by the alignment algorithm as the tracking is invariant under these transformations. There are also more subtle modes which affect the momentum but not the residual distributions. This challenge is explored in more detail in section 8. Thirdly, as the alignment algorithm is located at the end of the data processing chain, from the actual particle hitting the detector to the reconstructed track, problems in the underlying infrastructure will certainly affect the measurement of the module positions.

7 Distributed Alignment

The Robust Alignment algorithm is suitable for distributed alignment. Thus, the calculation of alignment constants may be performed on many sub-samples of the input data using several computers simultaneously. In each iteration the reconstruction of the events in each of the sub-sample produces a file with alignment information. In a second step these files are merged and alignment constants calculated. This feature is fully implemented in the ATLAS offline software [2] and has already been used and tested successfully [3].

8 Sagitta Distortions

Any track based alignment algorithm is designed to measure the relative module positions by optimising track parameters. However, it is known that there are global deformations of the detector, so called weak modes, that do not have any impact on the quality of the track parameters.

Tracking is invariant under global translation and rotation. However, if the real origin (x, y, z) of the tracks is known it can be compared with the mean values, x' , y' and z' , of the vertex distribution. If (x, y, z) does not match (x', y', z') , the Robust Alignment algorithm is able to perform a global transformation T which is given by

$$T = (x - x', y - y', z - z'). \quad (23)$$

Applying this correction is particularly important for a correct measurement of the impact parameter d_0 .

Special care has to be taken of systematic rotations of individual detector barrels which only affect the reconstructed particle momentum, but not any other parameter. Further examples of possible modes are described in Ref. [4]. There are generally three classes of solutions to this problem. Firstly, it is possible to constrain the momentum of the particle tracks used for the alignment. Reconstructing particle tracks, especially those originating from cosmic rays, in runs without any applied magnetic field produces straight tracks, which is equivalent to having tracks with infinite momentum. Thus, the momentum is

naturally constrained. Other suggested solutions include momentum constraints from invariant mass measurements on known resonances and using the TRT to give an estimate of the momentum. Secondly, tracks from cosmic rays - even with magnetic field - correlate the upper and the lower part of the detector and thus, constrain certain global modes. Thirdly, it is possible to use the Calorimeter information to detect global sagitta distortions. With asymmetries between the E/p ¹⁾ distributions from electrons and positrons it is possible to measure certain distortions independent of the Calorimeter calibration [4].

The first and second solution are naturally implemented in the Robust Alignment algorithm and have already partly been tested successfully. For example, tests with the Combined Test Beam showed that the correct momentum scale can be recovered if the momentum of a certain class of particles is known. The third solution requires a completely independent algorithm which translates the information from the E/p distributions into alignment constants.

9 Removal of Edge Channels

An edge channel is defined as the strip or pixel that forms the border of an SCT or PIXEL module. Due to the thickness of the silicon wafer, the measured interaction point of the track with the silicon may lie outside of the active material if the track is not perpendicular to the module. This biases the residual measurement. Furthermore, charge generated by the particle may induce a signal in the neighbouring strip if the track is close to the edge of the main strip. For edge channel strips this is, however, not possible and again the residual measurement becomes biased [5]. Tracks going through two overlapping modules hit edge channels more frequently which affects the overlap residual measurement significantly (Fig. 3). Additionally, if there is a bias in both hits of the overlap residual, the biases are of opposite sign. Thus, the bias of the overlap residual is twice as big as that of the residual measurement. Therefore, it is necessary to remove edge channels, even though it reduces the number of overlap hits significantly²⁾.

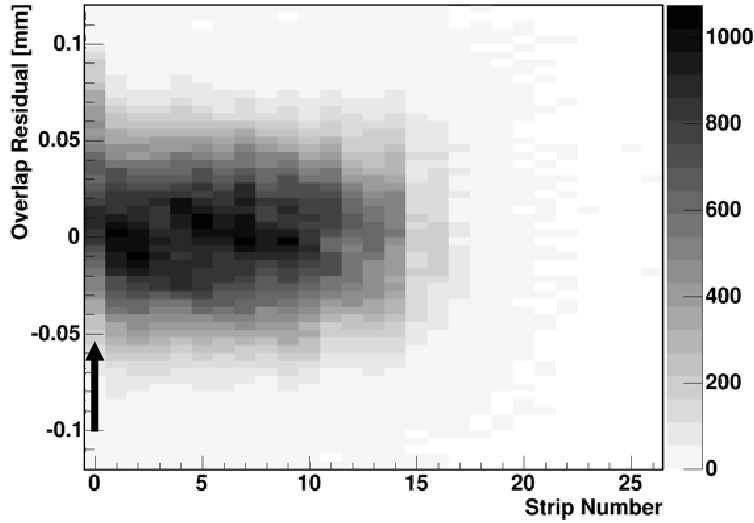


Figure 3: Overlap residual distribution as a function of the SCT strip number for all SCT barrels. The strip number is given for the hit closest to the edge of the module. Only the strips which form overlaps are presented. Channel 0 shows a positive bias.

¹⁾ E/p is the measured energy to momentum ratio.

²⁾Reduction between 6% for SCT local X overlaps to 100% for the central PIXEL local Y overlaps.

10 Effect of Multiple Scattering on SCT Local Y Residuals

Each charged particle traversing through the tracking detector is deflected mainly by small-angle Multiple Coulomb Scattering (MCS) off nuclei. MCS affects the tracking resolution and is most significant for low momentum tracks. Neglecting the uncertainty on the track fit, the measured width σ of the residual distribution is a function of the intrinsic resolution δ_{res} and the average deflection due to MCS δ_{MCS} :

$$\sigma^2 = \delta_{res}^2 + \delta_{MCS}^2 \quad (24)$$

Generally, the size of the average deflection δ_{MCS}^2 does not depend on the direction X or Y as the scattering in the silicon occurs symmetrically in all directions. It is, however, not correct to assume that the SCT detector can be considered as a simple PIXEL-like detector in which Eq. 24 still holds. Due to the two strip detectors geometry of the modules, their particular placement in the different layers of the SCT and the design of the tracking algorithm, the effect of MCS is much higher than Eq. 24 would suggest. As the Robust Alignment algorithm is the only ATLAS algorithm which analyses the SCT local Y residuals, this phenomenon was unknown prior to this analysis. In the following, a simple model is presented which correctly predicts the magnitude of the observed increase in the local Y resolution.

The ATLAS tracking algorithms reconstruct tracks by minimising all 3-dimensional distances between the track and the strips. These strips belong to modules which are rotated from layer to layer by alternately ± 20 mrad around the local Z axis. In order to estimate the magnitude of this effect it is useful to make a simple, but general model [3] which assumes the tracks to be perpendicular to the module planes. One module in each of two layers is sufficient for this purpose. Both modules are rotated with respect to each other by an angle α in the plane perpendicular to the track. Here, α is equal to the stereo angle between the two wafers of each SCT module.

Assuming that the particle undergoes MCS only between the two hits in the respective modules, two cases are possible: a scatter in the local X or local Y direction. In the first case, due to geometrical effects, a scatter δ_x in local X leads to a change in the local Y position of

$$\delta_y = \frac{\delta_x}{2 \cdot \tan(\alpha)}. \quad (25)$$

This term is added to the contribution from local Y scatters. Thus, the effect of MCS on the local Y resolution gets magnified by a factor M which can be approximated by

$$M = \sqrt{\frac{1}{4 \cdot \tan^2(\alpha)} + 1}. \quad (26)$$

For small angles α the first term is much greater than the second. For the ATLAS SCT α is 40 mrad. With this model there is an increase of the MCS effect by a factor of approx. 13. Simulation studies with single muon tracks were performed to test this simple model. A low and a high energy sample which contained only muons with momenta greater than 200 MeV and 20 GeV, respectively, were used. Using Eq.24 and assuming that MCS above 20 GeV is negligible, an average δ_{MCS} of almost $80\mu\text{m}$ for tracks above 200 MeV was found by measuring the local X resolution σ in both samples. By applying then the same calculations to the local Y residual distributions in both samples, a factor M of about 14 was measured. Hence, this simple model predicts the correct order of this effect.

The residual measurement in the local X direction is slightly magnified due to MCS in the local Y direction. However, this effect is only of the order 10^{-5} :

$$M = \sqrt{\frac{\tan^2(\frac{\alpha}{3})}{4} + 1}. \quad (27)$$

This model suggests that the magnification of MCS effects would neither exist if tracks were reconstructed by minimising all 3-dimensional distances between the track and the 2-dimensional space points made out of two strips, nor would it be there if the modules had the same orientation in each layer. In the latter case minimising all 3-dimensional distances between the track and the 2-dimensional space points gives the same result as minimising the distances to all strips individually.

11 Combined Test Beam Alignment

The ATLAS Combined Test Beam (CTB), which took place at CERN using the H8 beam line, was a test of final prototypes of the detector elements which had similar performances to those installed in the full ATLAS detector. Its aim was to represent a slice of the full ATLAS detector at $\phi = 90^\circ$ and $\eta = 0.0$ containing elements of the Inner Detector, the Calorimeter and the Muon detectors. The data used in this study was collected in October and November 2004 after the installation of the PIXEL and SCT modules. The coordinate system was chosen to be right handed with the x-axis in beam direction and the y-axis vertically towards the sky. The CTB Inner Detector consisted of three sub-detectors: PIXEL, SCT and TRT. The PIXEL detector was made of six modules, two in the PIXEL B layer and two each for PIXEL layer 1 and 2. The active surface of each module was $z \times y = 60.8 \times 16.4 \text{ mm}^2$. There was an overlap of about 2 mm between the two modules in each layer. The SCT detector consisted of four layers with two modules per layer covering each an area of $z \times y = 120.0 \times 60.0 \text{ mm}^2$. There was a 4 mm overlap between the two modules in each layer. Although the CTB setup approximately represented a slice of the full ATLAS detector, SCT endcap instead of barrel modules were used.

The Robust Alignment aligned all 14 CTB modules successfully in the local X and Y direction [6]. The algorithm converged quickly to a stable solution without applying any alignment specific track selection. For the alignment presented 72 553 events with 100 GeV pions unexposed to a magnetic field were used. Although the alignment was performed with only one run, the final alignment constants were also valid for all other runs, with or without magnetic field. The Robust Alignment succeeded improving the residuals significantly as can be seen in Fig. 4. Some of the CTB modules were mounted by hand which introduced much larger tilts than there are expected for the full ATLAS detector. Therefore, after alignment the hit residuals are partly still larger than it is expected from simulation.

12 SCT Alignment With Cosmic Ray Tracks

The first test of the SCT barrel with cosmic ray muons was performed on the surface inside the SR1 building at CERN. The whole setup consisted of all four SCT barrels, the TRT and three scintillator layers which were used to trigger cosmic ray events. Only part of the SCT and TRT was connected to the read out system. In total 467 SCT modules and 24 TRT modules were used to measure tracks from cosmic rays. Due to a 15cm layer of concrete, muons with momenta smaller than approx. 100 to 200 MeV did not reach the lower trigger. The collected data sample contains only tracks from muons which did.

The Robust Alignment algorithm successfully aligned all 467 modules of the SR1 SCT setup in the local X and Y direction. The algorithm converged to a stable solution without any alignment specific track selection. The final alignment constants improve the residual and overlap residual distributions significantly (Fig. 5). After alignment, the distributions are much narrower and nicely centered around zero. The layer and side dependence of the residual widths is caused by MCS and also appears in simulated data. For the alignment presented, 200 000 events collected in 13 runs were used. This dataset is about half of the available sample and is sufficient to produce alignment constants with a statistical uncertainty of mostly 1 μm in local X and about 40 μm in local Y. The alignment using the SR1 data was

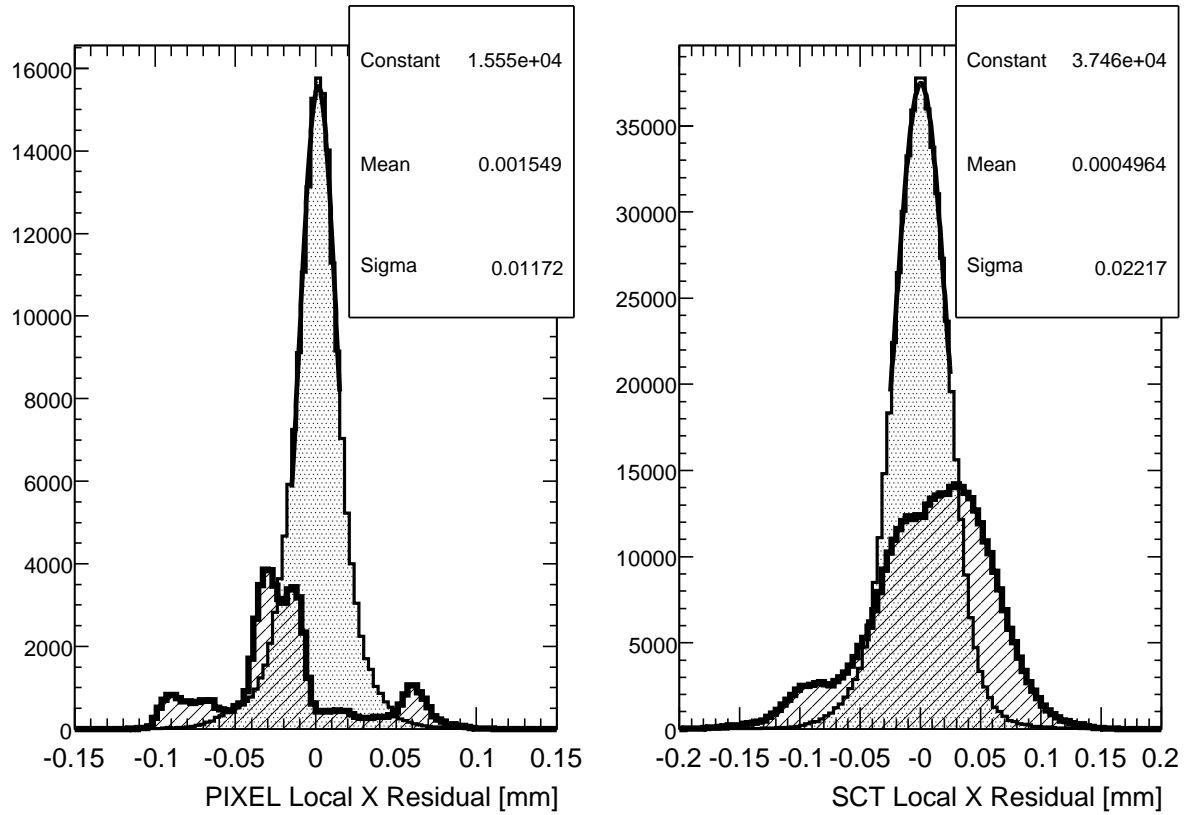


Figure 4: The local X residual distributions for the CTB PIXEL (left) and SCT (right) detector are shown: Initial alignment (dashed area) and after robust alignment (dotted area) with run 2102355.

performed with distributed alignment. Neglecting the waiting time for the CERN batch system an overall integrated time of about 34 hours with 10 CPUs was used for the alignment. However, already after 5 hours good alignment constants were produced. The final 50 iterations which lead to full convergence only improved the resolution by a few microns.

13 CSC Alignment

In order to study scenarios where all modules are randomly displaced and understand the effect of systematic distortions to detector subsystems, such as the individual SCT and PIXEL barrels or endcap disks, data samples were simulated with an “as built” geometry and a distorted magnetic field [7]. The alignment studies (only one example is presented) are part of the ATLAS Computing System Commissioning (CSC) and Calibration Data Challenge (CDC). In Fig. 6 the Robust Alignment performance for the local X alignment of SCT barrel 0 is shown. This study was performed on the level of local misalignments using events with ten muons each³⁾. In the CSC geometry, this SCT barrel has random displacements between $\pm 150 \mu\text{m}$. After Robust Alignment most of these displacements were recovered. The remaining difference between the actual CSC geometry and the Robust Alignment constants is on average about $20 \mu\text{m}$. This difference is caused by statistical effects, module rotations and remain-

³⁾The energy of these muons is equally distributed between 2 GeV and 50 GeV with a η -range of ± 2.7 .

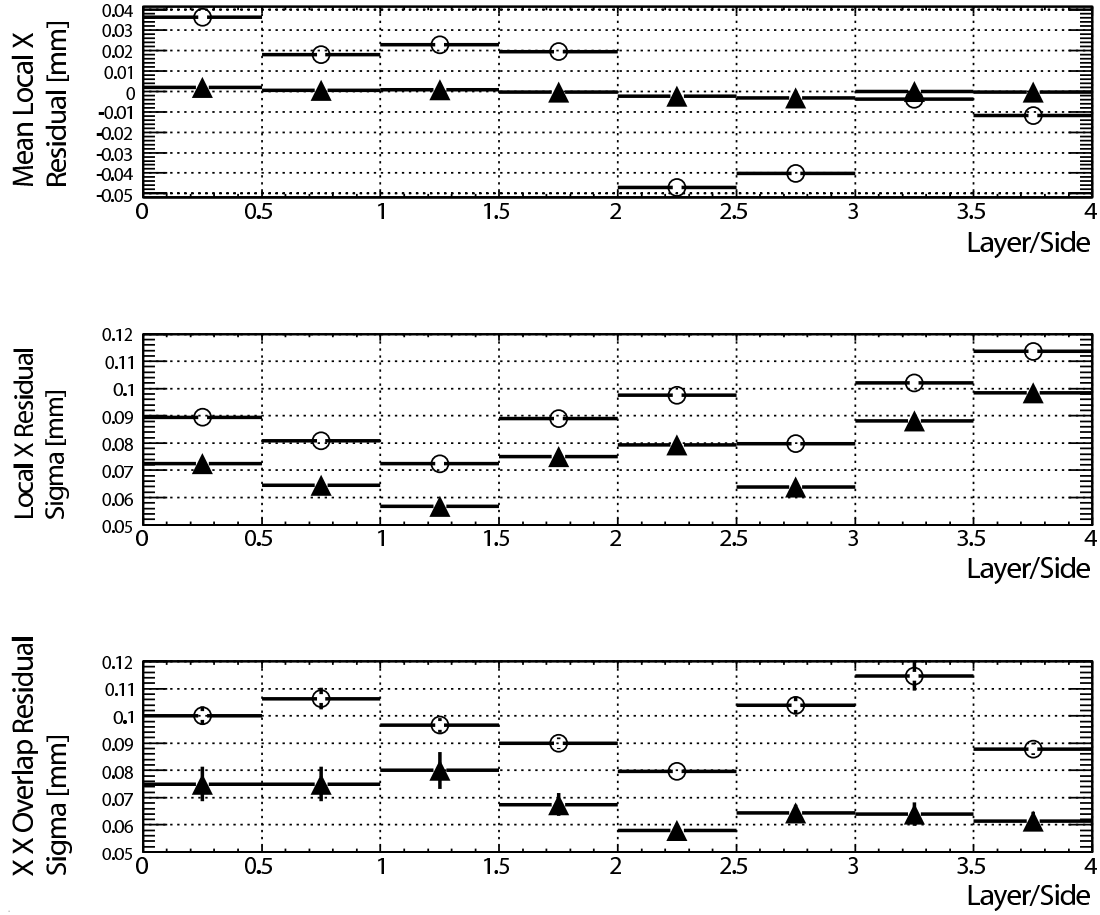


Figure 5: Top: The mean SCT local X residuals are shown for each layer and side before (white circles) and after Robust Alignment (black triangles). Middle: The unbiased SCT local X residual widths are shown for each layer and side before (white circles) and after Robust Alignment (black triangles). Bottom: The biased SCT local X local X overlap residual widths are shown for each layer and side before (white circles) and after Robust Alignment (black triangles).

ing systematic global distortions. With these alignment constants, residuals, track parameters and track efficiencies are significantly improved. Studies including global distortions showed a similarly good performance of the Robust Alignment algorithm. However, other methods will be required to fully remove some of the remaining sagitta distortions.

14 Summary and Conclusion

A robust track based alignment method using residuals and overlap residuals has been presented. This algorithm is numerically very stable as no matrix inversion or minimisation is involved. Therefore, good results were achieved in all cases without any alignment specific track selection. It is designed to align the ATLAS silicon tracking detectors with collision data, especially when the experimental conditions are not yet well known. Furthermore, it is ideal for performing simple and independent cross checks to other alignment algorithms. In addition to radial corrections it only measures misalignments in the direction of the two most important degrees of freedom: the local X and Y coordinates. These variables

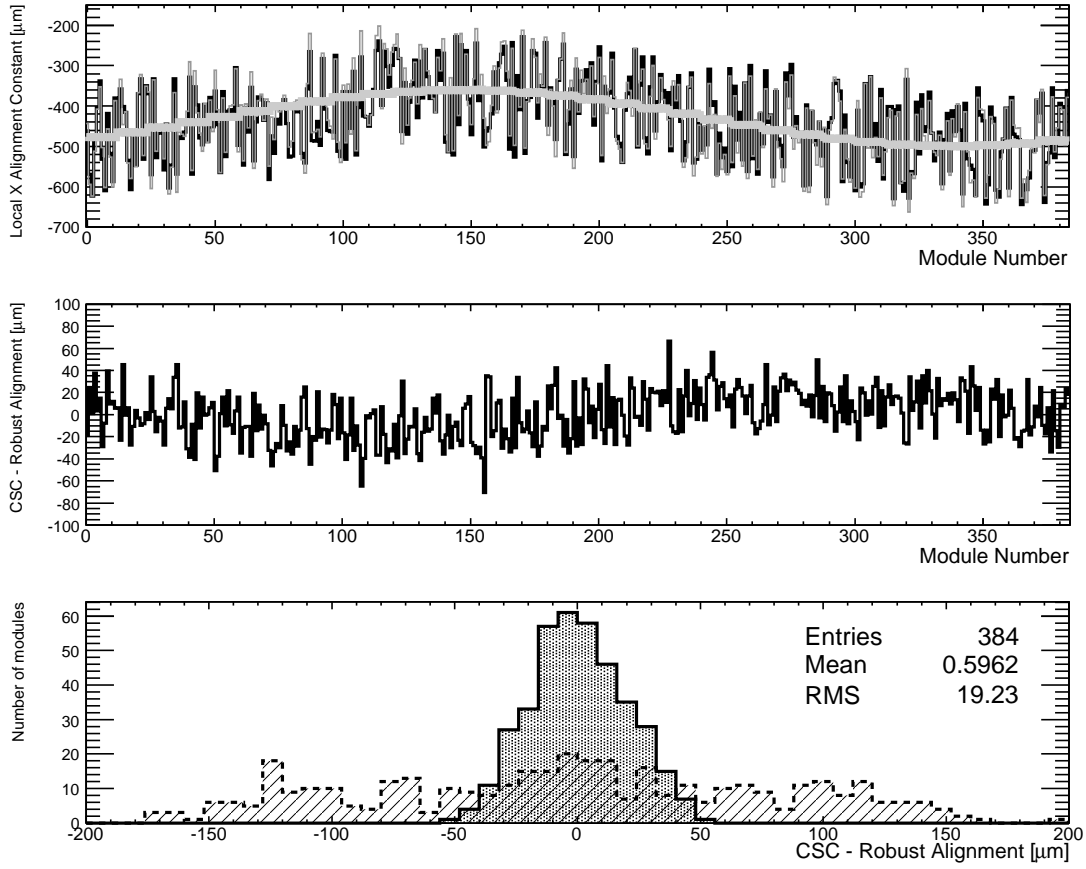


Figure 6: Alignment results for SCT barrel 0 are shown. Top: Alignment constants for CSC geometry (black), CSC global misalignments (thick light grey) and Robust Alignment (thin grey). Middle: Difference between CSC geometry and Robust Alignment constants. Bottom: Difference between CSC geometry and Robust Alignment before (dashed) and after (dotted grey area) alignment.

are crucial as they have the most impact on the track properties. Tests showed that, in the local X and Y direction, the Robust Alignment is able to determine alignment constants of similar quality than those from the other two ATLAS track based alignment algorithms. The Robust Alignment algorithm has been successfully implemented into the official ATLAS offline software and is fully operational. The method presented is very general and can be used for the alignment of any other silicon tracking detector with overlapping modules.

15 Acknowledgements

This work has been performed within the ATLAS Collaboration and I would like to thank collaboration members for great support. Especially, my thanks go to the ATLAS Inner Detector alignment group, lead by Dr. Jochen Schieck and Dr. Salva Marti, for many fruitful discussions and to Dr. Tony Weidberg for excellent supervision. Furthermore, I would like to thank Helen Hayward and Kathrin Stoerig for plots and the Oxford alignment group, namely Dr. Pawel Bruckman de Renstrom, Dr. Muge Karagoz-Unel, Ellie Dobson, Oleg Brandt, Dr. Stephen Gibson and Dr. Alessandro Tricoli.

References

- [1] ATLAS Collaboration, ATLAS Inner Detector, Technical Design Report Volume 1, in ATLAS TDR 4, (CERN/LHCC 97-16, 1997).
- [2] ATLAS Computing group, ATLAS Computing, Technical Design Report, in ATLAS TDR 17, (CERN/LHCC 2005-22, 2005).
- [3] F. Heinemann, Robust Track Based Alignment of the ATLAS Silicon Detectors and Assessing Parton Distribution Uncertainties in Drell-Yan Processes, PhD Thesis, University of Oxford, In preparation for 2007.
- [4] D. Hindson, A Robust Procedure For Alignment Of The ATLAS Inner Detector Using Tracks, PhD Thesis, University of Oxford, 2004.
- [5] F. Campabadal et al., Nucl. Inst. & Meth. in Phys. Res. A **538** (2005) 384–407.
- [6] S. Gonzalez-Sevilla et al., ATL-COM-INDET-2007-013 (2007).
- [7] A. Ahmad et al., ATL-COM-INDET-2007-012 (2007).